Spray Cooling Using Multiple Nozzles: Visualization and Wall Heat Transfer Measurements

Bohumil Horacek, Jungho Kim, and Kenneth T. Kiger

***Abstract*—Time- and space-resolved heat transfer data on a nominally isothermal surface, cooled by two spray nozzles, were obtained using an array of individually controlled microheaters. Visualization and measurements of the liquid–solid contact area and three-phase contact line length were made using a total internal reflectance technique. The spacing between the nozzles and the heated surface was varied between 7 and 17 mm. Little interaction between the two sprays was observed for the tested conditions, with the heat flux due to a single nozzle remaining comparable to that due to two nozzles, provided the areas considered were limited to the regions impacted by the sprays. Variations in the heat transfer across the surface, however, increased significantly with decreasing nozzle-to-heater spacing. The phase change heat transfer was strongly correlated with the length of the three-phase contact line and was not correlated with the wetted area.**

***Index Terms*—Contact line, multiple nozzles, phase-change heat transfer, spray cooling.**

NOMENCLATURE

CHF	Critical (maximum before dryout) Heat flux [W/m^2].
d_{32}	Sauter mean diameter [m].
d_0	Spray nozzle diameter [m].
$f\#$	f-number; as given by the ratio of an imaging len's focal length to clear aperture.
$G_{i,j}$	Normalized gray value of a single pixel at position (i, j) in a 2-D image.
$G_{\mathrm{min,j}}$	Minimum of (the smallest gray value along jth row) or 0.45.
$G_{\mathrm{max},j}$	Maximum of (the largest gray value along jth row) or 0.65.
h	Nozzle to heater distance [m].
i	index in x-direction.
j	index in y-direction.
L_c	Contact line length [m].
n	Index of refraction.
Re	Reynolds number.
T_{sat}	Saturation temperature [°C].
T_w	Heater temperature [°C].
v	Velocity [m/s].
We	Weber number.

Manuscript received September 1, 2004; revised September 11, 2004. This work was supported by the Laboratory for Physical Sciences (LPS), College Park, MD, under Grant MDA90499C2618. This paper was originally presented at the 2004 ASME Heat Transfer/Fluids Engineering Summer Conference, Charlotte, NC, July 2004.

B. Horacek is with Degussa Construction Chemicals, Ltd., Chrudim, Czech Republic.

J. Kim and K. T. Kiger are with the Department of Mechanical Engineering, University of Maryland, College Park, MD 20742 USA (e-mail: kimjh@umd.edu).

Digital Object Identifier 10.1109/TDMR.2004.838399

Symbols

ΔP	Pressure drop [Pa].
μ_f	Dynamic viscosity of liquid [Pa·s].
ρ_a	Density of ambient [kg/m^3].
ρ_f	Density of liquid [kg/m^3].
σ	Surface tension [N/m].

I. INTRODUCTION

SPRAY cooling can be used to transfer large amounts of energy at low temperatures by utilizing the latent heat of evaporation of the working fluid. Heat transfer rates much higher than can be attained in pool boiling (typical CHF for pool boiling of FC-72 is $\sim$ 16 W/cm^2) are possible with sprays, since the vapor is not hindered by a bulk pool of liquid and can be more readily removed from the heated surface. Heat fluxes as high as 1000 W/cm^2 have been observed in gas-assisted spray cooling with water [1], [2]. Up to 100 W/cm^2 have been observed using FC-72 [3]–[5]. As a result, such techniques have recently seen a renewed interest in electronic cooling applications. Because of its efficiency and ability to isothermally remove heat, spray cooling is a leading candidate to cool high-power diode laser arrays in terrestrial environments, and has potential for cooling future space-based laser (SBL) and space-based radar (SBR) devices. Spray cooling is also currently being used in production commercial applications, with the latest example being the Cray X-1 supercomputer. Use of a low-temperature boiling point dielectric liquid compatible with electronics (e.g., fluorocarbons) is an attractive option with this technology, as it allows direct cooling of the components, eliminating the thermal contact resistance between the heat sink and the chip that exists with conventional methods, such as finned heat sinks.

Although a significant amount of research has been performed with single nozzles and surfaces with small areas ($\sim$ 1.6 cm^2 and smaller) (e.g., [3]–[10]), or cooling of large areas (59 cm^2) with a single nozzle at low heat flux (13 W/cm^2) [10], cooling of large surfaces with high heat flux will require use of multiple nozzles. Very little data is currently available on multiple nozzle heat transfer. Recently, spray cooling curves using an array of 4 $\times$ 12 nozzles to cool a heated 25.4 mm $\times$ 76.0 mm copper block were obtained [11]. The critical heat flux (CHF) for this array (19.3 cm^2) was found to be 34% lower than that on a 2.0 cm^2 heater cooled by an 8-nozzle array. The authors speculated that the lower heat transfer resulted from accumulation of excess liquid in the central region of the heated surface due to the impedance created by the impacting sprays nearer to the outer edges of the heated surface.

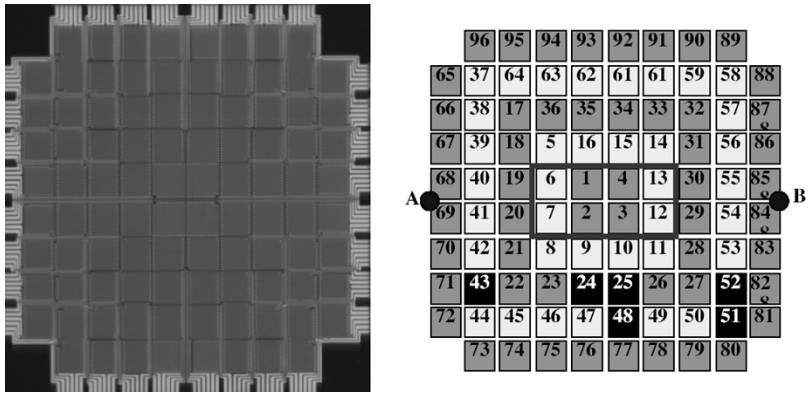

(a) (b)

Fig. 1. (a) Photograph of heater array and (b) schematic of heater numbering. The impact locations of nozzles A and B (black circles) and the area imaged for the total internal reflectance technique (rectangle enclosing heaters 1, 2, 3, 4, 6, 7, 12, and 13) are indicated. Inoperable heaters are colored in black.

Since the above studies were limited to space-averaged heat transfer measurements and no visualization was performed, many questions persist regarding the impact multiple nozzles have on heat transfer distribution and droplet interaction. The heat transfer at the stagnation region close to the plane of symmetry between nozzles may be significantly lower than in other parts of the spray, resulting in nonuniform temperature distributions on the substrate. However, if the nozzle is placed further from the surface, and if the spray is sparse, the overlap between sprays may not result in a stagnation region being formed.

The purpose of this research was to determine how the heat transfer from flat surfaces is altered by spray interaction when two nozzles instead of one are used to cool the surface as the spray nozzles were traversed away from the heated surface. Two very powerful techniques were used to quantify the heat transfer behavior: 1) the space resolved heat transfer distribution was measured using an array of individually controlled microheaters (each heater in the array was kept at constant temperature using an electronic feedback circuit, and the instantaneous power required to do this was measured), and 2) the use of a semi-transparent heater surface allowed for visualizations of the liquid–solid contact area using a total internal reflectance (TIR) technique.

II. Experimental Apparatus

A. Heater Design

The heat transfer distribution produced by two nozzles was studied using two full cone ISR spray nozzles to cool a microheater array with a total area of 0.49 cm^2 (7.0 mm $\times$ 7.0 mm). The heater array consisted of 96 heaters each nominally 700 μm in size, similar to that used previously [4], [5]. A picture of the heater array is shown in Fig. 1, along with a schematic showing the heater enumeration and the location of inoperable heater elements that occurred during the fabrication process. Each heater element consisted of a thin (200 nm thick, 7 μm wide) serpentine platinum resistance heater that was sputtered onto a titanium adhesion layer on a 500 μm thick silica substrate. The effective temperature coefficient of resistance of the metallic layer was approximately 0.002 $^{\circ}C^{-1}$, with the length, width, and thickness of the serpentine elements designed to provide a nominal

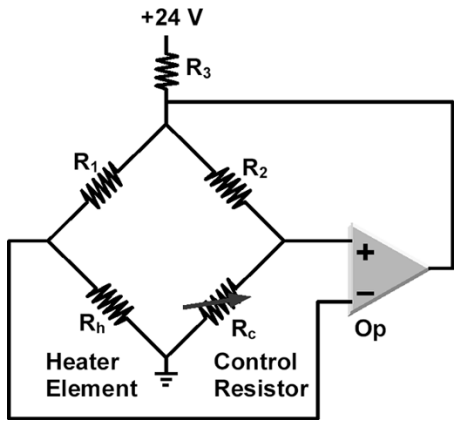

Fig. 2. Schematic of feedback control circuit for individual heater element.

resistance of approximately 180 Ω for each heater in the array. Thicker gold leads were deposited up to the edge of the array to ensure minimal lead resistance ($< 1\ \Omega$), and the entire array was covered with a 1-μm SiO_2 passivation layer to provide a uniform surface energy.

Individual heater elements were maintained at a constant specified temperature through the use of 96 separate Wheatstone bridge feedback circuits, one of which is illustrated schematically in Fig. 2. The temperature of the element was selected through the use of a 20 kΩ digital potentiometer with 512 discrete steps. When combined with the other resistor elements in the circuit, the array temperature could be set from 30 °C to 110 °C with a resolution of approximately 0.2 °C. The frequency response of the combined heater/bridge circuit was approximately 15 kHz. In the current configuration, each heater was capable of dissipating 1.3 W, giving a maximum surface heat flux of up to 250 W/cm^2. The settings for the digital potentiometer were calibrated using a constant-temperature, insulated, calibration oven. A feedback controller was used to maintain a constant interior oven temperature, while the threshold setting of the digital potentiometer that just started regulation of the circuit was determined. The calibration was performed on each of the heater elements in 5 °C increments between 30 °C to 100 °C. During the experiments, two 64-channel 12-bit analog-to-digital conversion boards were used to sample data from each individual heater at 500 Hz.

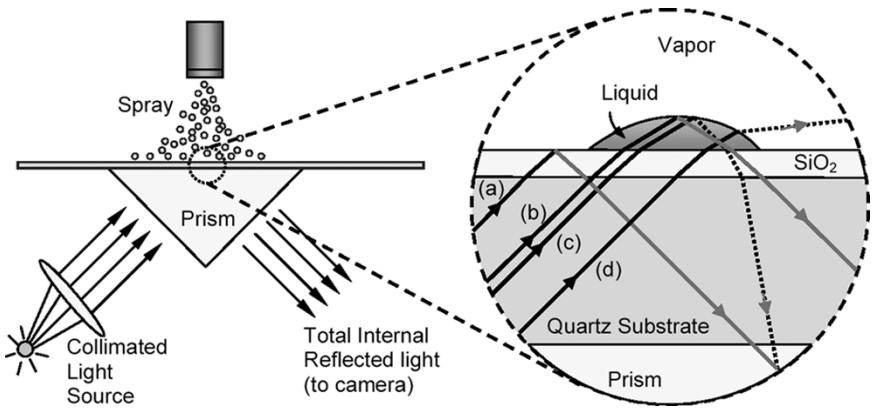

Fig. 3. Schematic of total internal reflectance (TIR) technique. Light incident at the SiO_2/vapor interface (a) undergoes a total internal reflection, while light incident on the SiO_2/liquid interface is transmitted (b–d). Most of the light (96%) striking the liquid/vapor interface is transmitted into the liquid and subsequently is scattered by a combination of reflection at a sloped interface (c) or refraction into the vapor (d). Places where the liquid surface is completely parallel to the SiO_2 surface will reflect the light to the camera, but these are typically confined to regions smaller than the image resolution.

B. Visualization Technique

The use of a transparent silica substrate combined with the 50% coverage area of the serpentine heater element allowed for visualization of the impacting spray from beneath the semi-transparent heater array. A high-speed digital camera (Vision Research Phantom v4.0) capable of acquiring 512 × 512 pixel images at speeds of up to 1000 fps was used to record the visualizations. For the current experiments, the camera was synchronized to the data acquisition system of the heater array. A telemicroscope lens (Infinity KC with IF3 objective) provided variable magnification imaging (0.9 x–1.3 x) with a working distance of 15–19 cm. The lens and camera were adjusted to provide a clear image of 8 heaters in a 2 × 4 formation on the array surface (heaters marked numbers 1, 2, 3, 4, 6, 7, 12, 13 in Fig. 1).

Areas of liquid-solid contact area were obtained using the TIR technique shown schematically on Fig. 3. The TIR technique has been used in the past to study sprays [5], pool boiling [12], [13], and droplet impact [14]. Details of the implementation of the method are provided below, and a review of the method can be found in [14]. A right angle prism (index of refraction, $n = 1.517$) was placed in contact with the underside of the silica substrate ($n = 1.544$) containing the heater array. An optical immersion oil ($n = 1.52$) was used to ensure no air gap existed between the prism and the substrate. Light from a collimated source was then positioned such that total internal reflection of the light occurred at the interface between the SiO_2 passivation layer ($n = 1.46$) and the vapor in the chamber ($n = 1.00$), resulting in a bright area on the image (see ray trace (a) in Fig. 3). The critical angle for total internal reflection from SiO_2 to a vapor is approximately 43°, which conveniently allowed the use of a 45° prism to direct the light into the substrate. If liquid was present, then the light traveled past the liquid–silica interface and was scattered at the liquid–air interface, forming a dark region on the image. A small percentage of light was reflected directly from the SiO_2/liquid interface, but calculations showed this to be less than 4% of the incident light. Due to the relatively small aperture and long working distance of the lens ($f\# \sim 10$), light that was scattered at the liquid–vapor interface but was not parallel to the lens axis was not imaged. The only exception to this was at locations where the slope of the interface was nearly parallel to the SiO_2 surface. For the small surface features observed under most conditions, these points were typically confined to regions below the resolution of the camera. An example of the type of image that can be obtained is shown on Fig. 4 under conditions where the wall temperature is close to CHF. The dark areas indicate liquid on the surface. As can be seen, the heater area covered by liquid and the length of the three-phase contact line (i.e., the curve where the liquid, vapor, and solid are in mutual contact on the heater surface, denoted in the text by L_c; see the last panel in Fig. 12 for illustration) can easily be determined with appropriate image processing (discussed below).

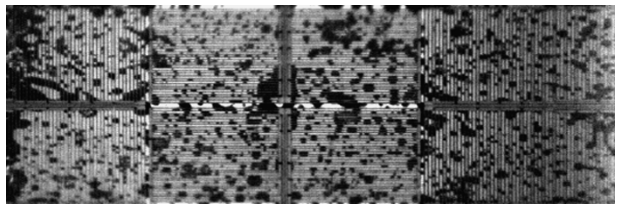

Fig. 4. Sample image obtained from the total internal reflection technique. The eight heaters [as outlined in Fig. 1(b)] are visible as faint horizontal or vertical stripes, while the wetted areas appear as black regions. Each of the above heaters is 700×700 mm^2.

C. Testing Protocol

The tests were performed within a closed flow loop consisting of a spray chamber, condenser, and pump (Fig. 5) with FC-72 as the test fluid. The FC-72 was distilled before placing it in the flow loop, and only fluid that evaporated between 56 °C and 60 °C was used in the tests. The test section dimensions were 25-mm wide, 16-mm high, and approximately 180-mm long. Temperature and pressure measurements were made at the inlet to the spray nozzle and within the liquid reservoir. Liquid flow through the spray nozzles were measured using two rotameters. The heater array was inclined at a slight angle with respect to the horizontal to help excess fluid that did not vaporize drain through the condenser into the reservoir. The nozzle distance from the heater surface (h) was varied from 7 to 17 mm.

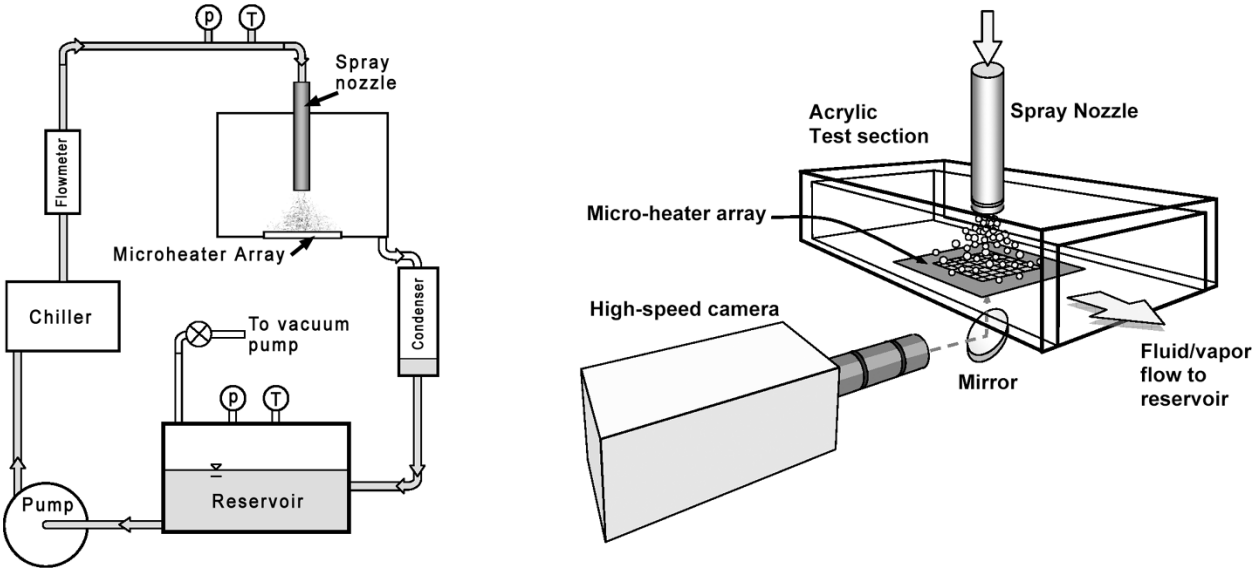

(a) (b)

Fig. 5. (a) Schematic of test loop facility and (b) detail schematic of test section, spray nozzle, heater, and high-speed camera.

The nozzle diameter was measured from magnified images to be $d_0 = 0.2$ mm. Two pumps could provide up 50 ml/min to each nozzle.

The pressure was kept at atmospheric pressure throughout the flow loop under all tested conditions by venting the reservoir to the ambient environment. No effort was made to degas the liquid. It has been shown [4], [5] that dissolved gas has the effect of subcooling the liquid being sprayed on the surface. Since the liquid temperature in the nozzle was nominally 25 °C and the boiling temperature of FC-72 at 1 atm is 56 °C, the spray was subcooled by nominally 31 °C.

III. Uncertainty Analysis

The uncertainties in the heat flux measurement result from a combination of losses to substrate conduction, inaccuracies in the calibration of the heater, and tolerances of the feedback circuitry, as described in detail in [4]. To avoid difficulties in accounting for conduction losses to the substrate at the edge of the heater array, the outer ring of heaters (Heater no. 65–96 in Fig. 1) were used as guard heaters. Data from these heaters are excluded from the calculations of the mean heat flux provided in the following section. The net resulting uncertainty in heat transfer due to measurement inaccuracies in the feedback circuit and data acquisition system can be conservatively calculated to be less than 3%.

Larger uncertainties in the spray cooling curve can result from uncertainties in liquid flow rate, wall temperature, and dissolved gas concentration. The liquid flow rate was steady to within 0.5 ml/min (1.4–4.5% over the range of flow rates tested). The uncertainty in wall temperature is assumed to be two positions on the digital potentiometer, or 0.4°C. The amount of gas in the flow loop can be determined by measuring the pressure and temperature in the flow loop. The *distribution* of the gas, however, can vary within the flow loop if the temperatures vary (as it does since the heater is hotter than the surroundings), making it difficult to quantify the local gas concentration. The accuracy of the pressure transducer used was 1.5%. Repeated measurements of the spray cooling curves under the same nominal conditions resulted in errors of about 4%. The total uncertainty in the spray cooling curves obtained by combining the uncertainty in repeatability with the measurement inaccuracies is estimated to be 5%.

IV. Results

Results were obtained with the spray nozzles oriented perpendicular to the plane of the microheater array, with a vertical separation of $h = 7$ to 17 mm from the surface as shown on Fig. 6. The horizontal spacing between the heaters corresponded to the microheater array width of 7 mm, enabling half of the spray from each nozzle to impact the heater when $h \leq 11$ mm. The horizontal nozzle spacing is constrained to a minimum of 7 mm owing to the diameter of the nozzle housing. The spray cone angle was measured to be about 32°, as indicated from side view photographs of the spray. No overlap between the two spray cones occurred for $h = 7$ mm, while the cases with $h = 11$ mm and $h = 14$ mm bracketed the ideal situation where the spray essentially inscribes the heated surface area resulting in maximum heat transfer [15]. Slight overlap between the sprays occurred for $h = 17$ mm. The flow rate through each nozzle was set at 30 ml/min, with about half of each nozzle flow impacting the heater for the 7–14 mm spacing. For the largest spacing of $h = 17$ mm, less liquid (approximately 11 ml/min) impacted the surface.

The size of the drops produced by the nozzle was estimated using a correlation for FC-72, FC-87 and water [16]

$$\frac{d_{32}}{d_0} = 3.67\left[We_{d_0}^{\frac{1}{2}}\mathrm{Re}_{d_0}\right]^{-0.259}$$

where $We_{d_0} = (\rho_a(2\Delta P/\rho_f)d_0)/\sigma$, $\mathrm{Re}_{d_0} = (\rho_f(2\Delta P/\rho_f)^{1/2}d_0)/\mu_f$. The mean absolute error of this correlation is claimed to be 12%. d_{32} (the average droplet diameter that has the same proportion of volume to surface

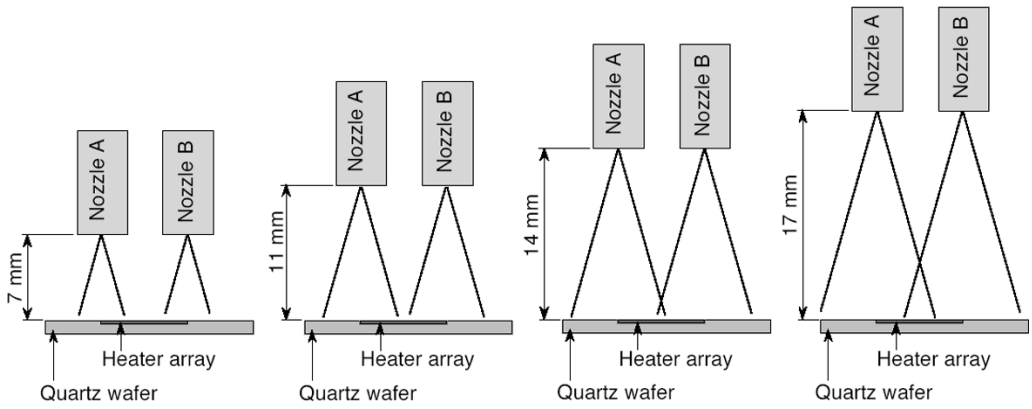

Fig. 6. Spray configurations studied. The spray angle is 32°, and the nozzles are spaced 7 mm apart.

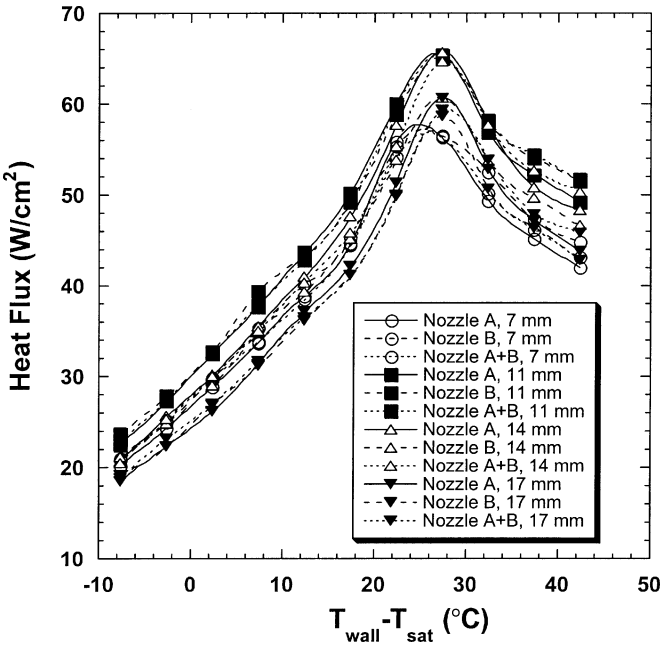

Fig. 7. Spray cooling curves for single nozzles, two nozzles. Note that the average heat flux for cases A and B is determined only from those heater elements located on the same half of the heater as the nozzle (i.e., left-half elements for Nozzle A, right-half elements for Nozzle B).

area as the original distribution of droplets) was computed from this correlation to be approximately 50 μm. An estimate of the droplet velocity impacting the surface, obtained from $v = \sqrt{2\Delta P/\rho_f}$, was 21 m/s for all cases.

A. Spray Cooling Curves

Spray cooling curves (heat flux versus wall superheat) were computed for the single nozzle cases by averaging the heat flux from only those heaters on the half of the array below the spray nozzle. For example, for nozzle A, only the heaters on the left half (Fig. 6) were included in the calculations. In a real system, a nozzle at the edge of an array would be positioned so that it does not cool more than the intended spray impact area, so only those heaters expected to be cooled by the nozzle are included in the area averaged heat flux.

The spray cooling curves for single nozzles and two nozzles are shown on Fig. 7. It is seen that the heat flux is similar regardless of whether one or two nozzles are activated. Even for the $h = 17$ mm case (where the sprays from the two nozzles overlap), the results are indistinguishable, which may be a result of the spray being "sparse," i.e., the droplets from adjacent nozzles do not interact with each other because their number density is low. The droplet flux onto the heated surface for sparse sprays is simply the sum of the droplet fluxes produced by two nozzles operating independently. If the sprays were not sparse, it might be expected that many of the droplets would collide with each other, altering the spatial droplet flux. The maximum heat fluxes occur for the $h = 11$ mm and $h = 14$ mm cases, as expected based on the spray coverage estimates.

The spray cooling curves indicate that the heat flux exhibits a linear dependence on the wall superheat at lower wall superheats, indicating that heat transfer occurs mainly through single phase convection in this region. It is only when the superheats become greater than about 17 °C does the two-phase convection become important (at least for the noncondensible gas concentrations used in the current experiments).

B. Heat Flux Distribution

The time-averaged spatial heat flux distribution is shown for several nozzle heights in Fig. 8. At the 7-mm spacing, the heat transfer is very high directly under the nozzle, but decreases rapidly away from the center of the nozzle impact site. As the nozzle distance is increased, the heat transfer across the array becomes increasingly more uniform. The heat flux uniformity can be quantified through the use of histograms as shown on Fig. 9, which shows the heat flux distribution as h is increased from 7 to 17 mm for a wall superheat of 23 °C. The histograms clearly indicate a decrease in the spatial variance as the nozzle is moved away from the surface. For example, the 25%/75% interquartile mean (IQM) and corresponding interquartile range (IQR) of the time-averaged heat flux spatial distribution for nozzle A as h is increased from 7 to 17 mm with $T_w - T_{\rm sat} = 23$ °C is 53 ± 49 W/cm^2 and 54 ± 10 W/cm^2, respectively. Thus, while the total rate of thermal energy removed from the surface is similar for these two cases, it is quite evident that the uniformity of the heat flux is vastly different. If uniform heat removal from the surface is desired, the spray flux density needs to be optimized (typically by specifying the nozzle, flowrate, and spacing from the surface).

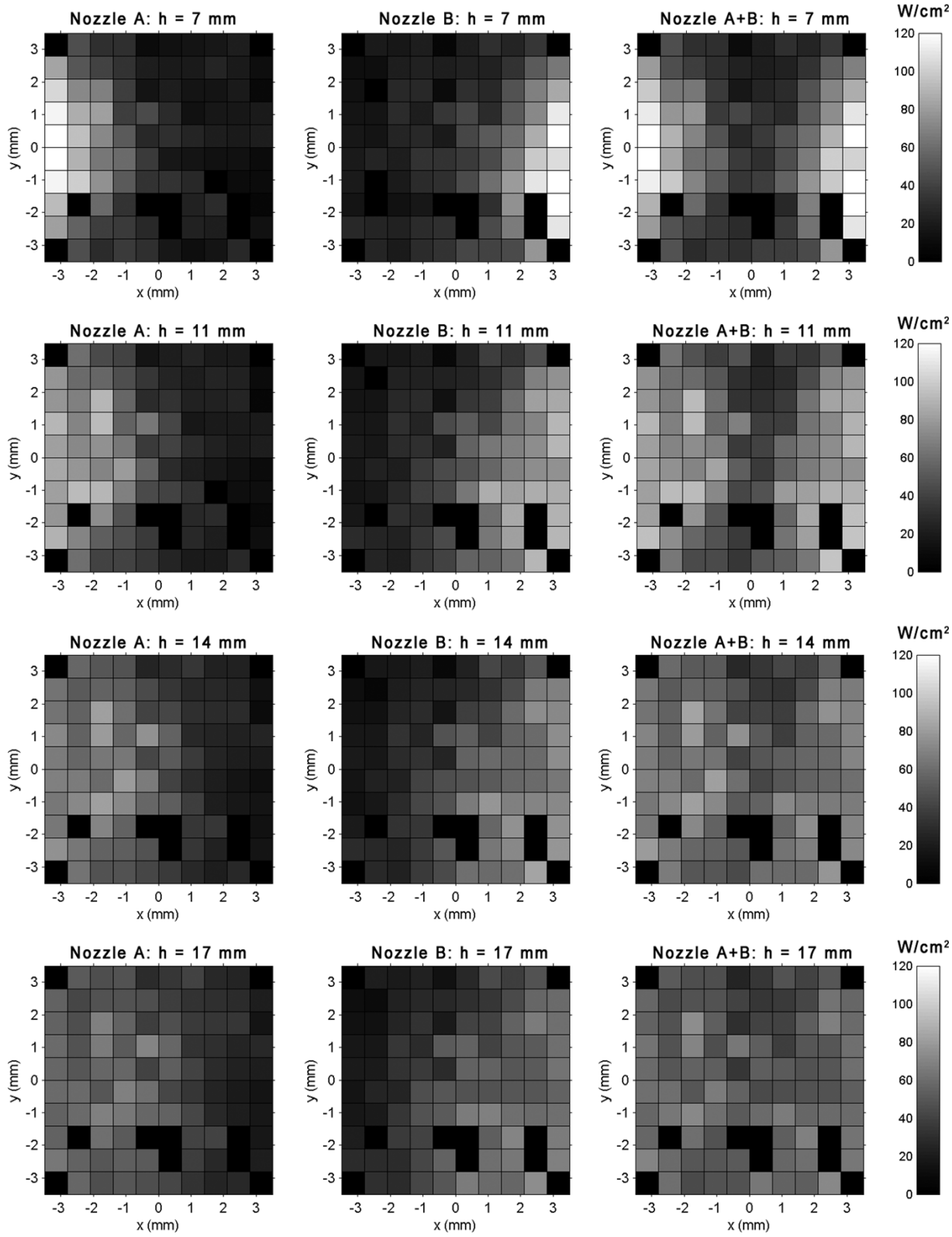

Fig. 8. Time averaged heat flux distribution across heater array at $T_w - T_{\rm sat} = 23\ ^\circ$C. The grayscale indicates heat flux in W/cm^2.

C. Visualization of Flow Structure

Figs. 10 and 11 show images obtained using the TIR technique for case B (single nozzle, right side) at several different nozzle heights above the heated surface and for several different wall surface temperatures. At low surface temperatures ($T_{\rm wall} - T_{\rm sat} < 10\,^\circ$C), the surface is covered by a thin, continuous liquid film. Transient, irregular streaks [Fig. 10(a), see white arrows] and circular or ring-shaped patterns [$T_{\rm wall} - T_{\rm sat} = -2\ ^\circ$C on Fig. 11(a) and (b); indicated by white arrows] are observed

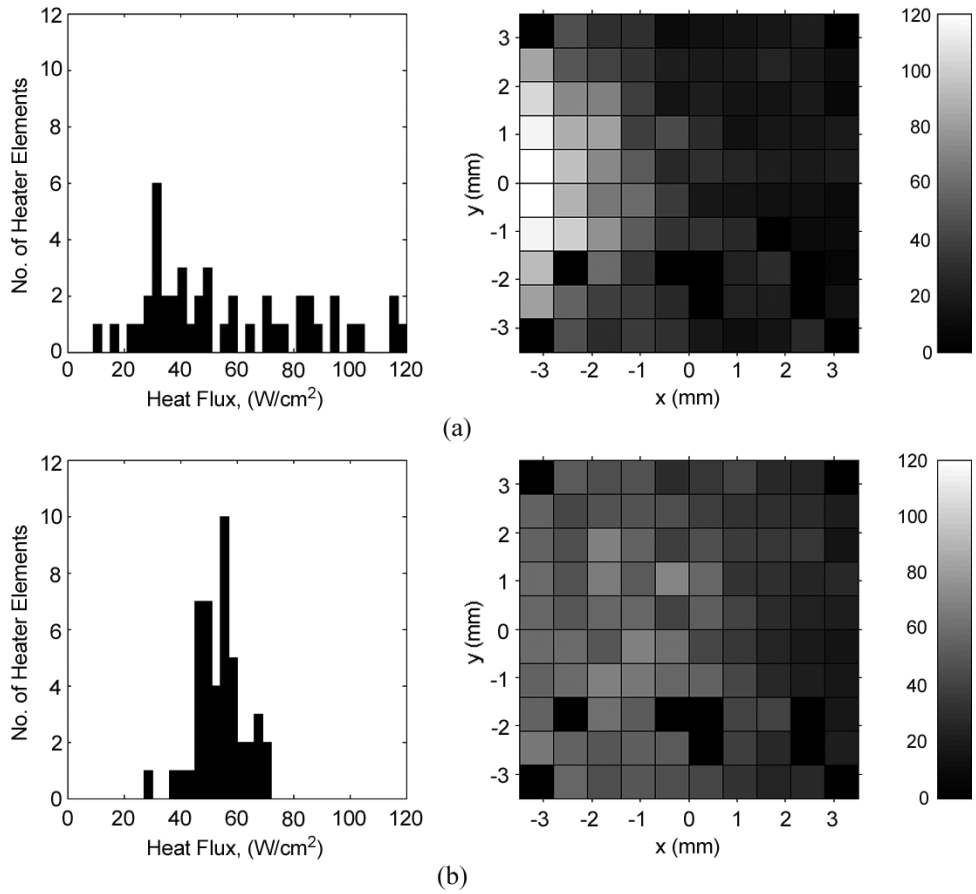

Fig. 9. Histograms of single nozzle heat flux at two nozzle-to-surface distances based on the left half of the array (nozzle A, 23 °C superheat). (a) $h = 7$ mm. (b) $h = 17$ mm.

to disrupt the homogeneity of the liquid surface film. The duration of these structures is difficult to track at the recorded temporal resolution (2 ms between frames), but typically they do not appear to persist for more than one image. Occasionally, however, a cluster of streaks can be observed to propagate across the field of view, moving away from the center of the spray impact region. These streaks likely correspond to capillary waves (i.e., small-scale free surface waves propagated by surface tension) generated by the shear of the entrained vapor in the spray as it is expelled away from the impact site. The circular and ring-shaped objects are thought to result from the impact of larger droplets with the liquid film, also generating capillary waves in the process. It is worth noting that virtually no circular/ring-shaped objects are observed at the lowest nozzle height [$h = 7$ mm, Fig. 10(a) and (b)], consistent with the fact that the spray is not impinging directly on the central eight heaters visible in the image. As the nozzle height is increased [Fig. 11(a) and (b)] the circular/ring disturbances begin to appear over a greater area of the image, indicating a corresponding increase in the direct spray coverage of the heater surface.

Once the wall superheat is increased above 10 °C, clearly visible dry spots begin to appear randomly on the surface. The spots are fairly round in shape and have high-contrast boundaries, indicating a clear demarcation between the wet/dry solid surfaces. The dry spots also do not appear to be localized at fixed positions on the substrate, as observed during the initiation of nucleate pool boiling, but instead occur at random locations on the surface and may disappear or move between successive images (2-ms framing rate).

With increased wall superheat under fixed spray conditions (nozzle height and flowrate), the number of dry regions tends to increase, with a gradual increase in the size of the largest spots [Fig. 10(b), $T_{\rm wall} - T_{\rm sat} = 17°{\rm C}$, $T_{\rm wall} - T_{\rm sat} = 22°{\rm C}$, $T_{\rm wall} - T_{\rm sat} = 27°{\rm C}$]. Above CHF, continuous bands of dry surface appear over several heaters as the remaining fluid forms rivulets streaming away from the impact site of the spray [Fig. 10(b), $T_{\rm wall} - T_{\rm sat} = 32$ °C]. Spatially, one can also discern differences in the wetted surface morphology as a function of the distance to the nozzle. The main difference is that the dryout regions appear larger with a reduced population of the smallest regions as one moves further away from the nozzle [moving from right to left in Figs. 10(b) and 11]. When quantitative values of the mean wetted area are examined (below), it is found that the spatial variation in wetted area is not significant among the different spatial positions (values are typically within 5% of each other across the face of the heating element). The contact length, however, is found to vary significantly as a function of position, which can differ by a factor of 2 during CHF conditions at low nozzle heights [Fig. 10(b), $T_{\rm wall} - T_{\rm sat} = 27$ °C].

As h is increased and more of the imaged heater array is directly impacted by the spray, a significant increase in the number of small dryout regions is observed, along with increased

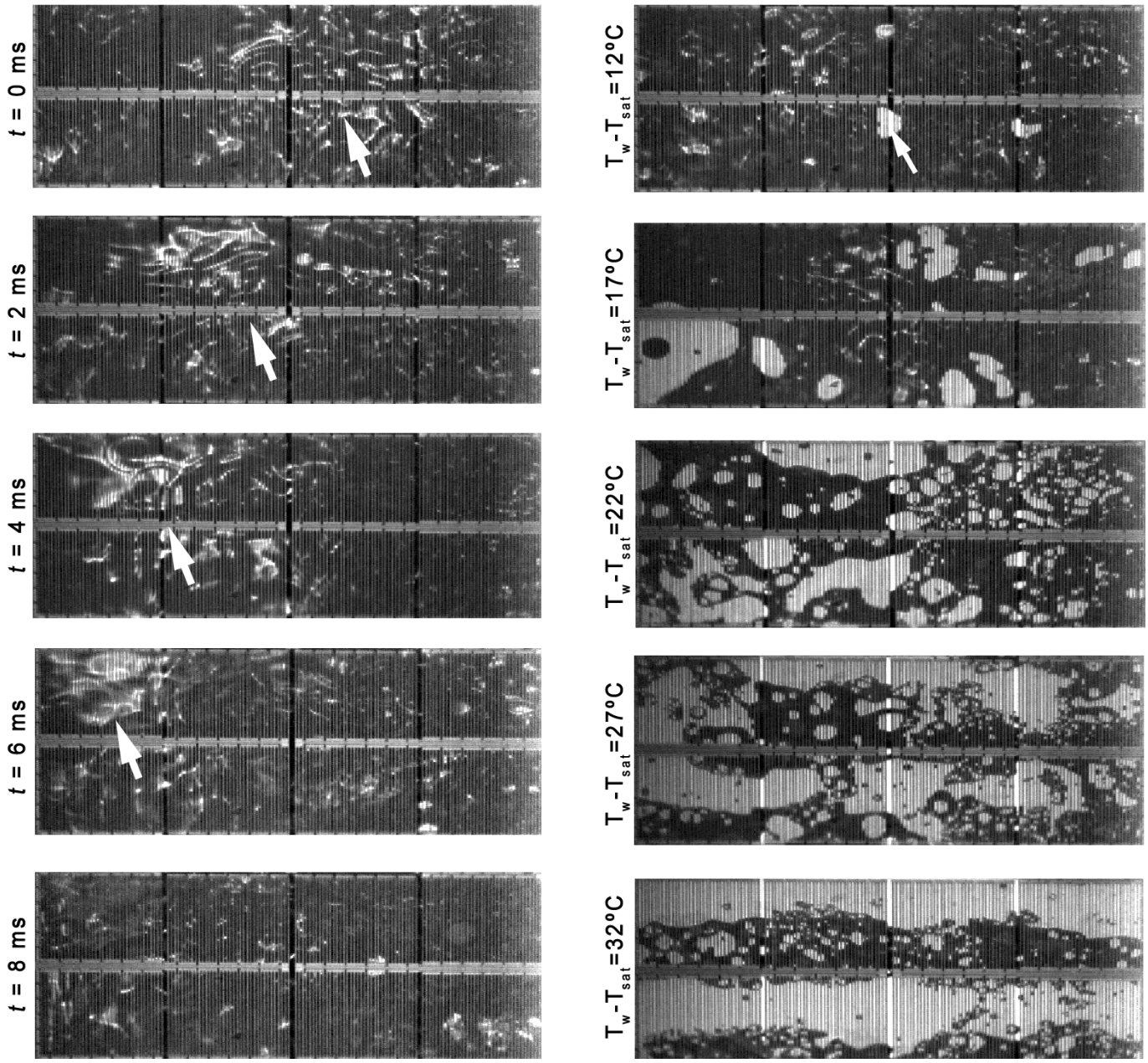

Fig. 10. (a) Sequence from $T_w = 50$, $h = 7$ mm showing surface wave disturbances propagating across heater surface (indicated by white arrow). Single nozzle activated (Nozzle B), with nozzle axis approximately 3 heater widths beyond the right edge of image. (b). Single images at various surface temperatures, $h = 7$ mm. Single nozzle activated (Nozzle B), with nozzle axis approximately 3 heater widths beyond the right edge of image. White arrow indicates a transcient dryout region for a low superheat case.

uniformity in the wetting of the heater surface [$T_{\text{wall}} - T_{\text{sat}} = 32$ °C on Fig. 11(a) and (b)]. For the heaters nearest the nozzle (right side of image), this results in a large initial increase in the heat flux, wetted area, and L_c $(h = 11$ mm$)$, followed by a gradual decrease in the heat flux and wetted area with further increases in height ($h = 14,\ 17$ mm), which is consistent with the fact that the $h = 11$ mm case is the first nozzle height in which droplets directly strike the heaters visible in the image (recall that the nozzle is centered approximately 2 mm beyond the right edge of the image). As the height is further increased, the spray density and impact velocity slightly decrease. For the regions furthest from the nozzle (left side of image), an increase in nozzle height results in a gradual monotonic increase in heat flux, the wetted area, and L_c. This is likely the result of a more gradual increase in drop impacts in this region compared to the region close to the nozzle.

D. Spray Cooling Heat Transfer Mechanism

L_c and wetted area were determined through image processing. In order to extract quantitative information from the images, the influence of the opaque heater lines must first be removed. For the magnification used in acquiring the images, the heater lines were approximately 1 pixel in width. A combination of a 2-pixel orthogonal line filter with a line-by-line renormalization was found to be effective in removing these

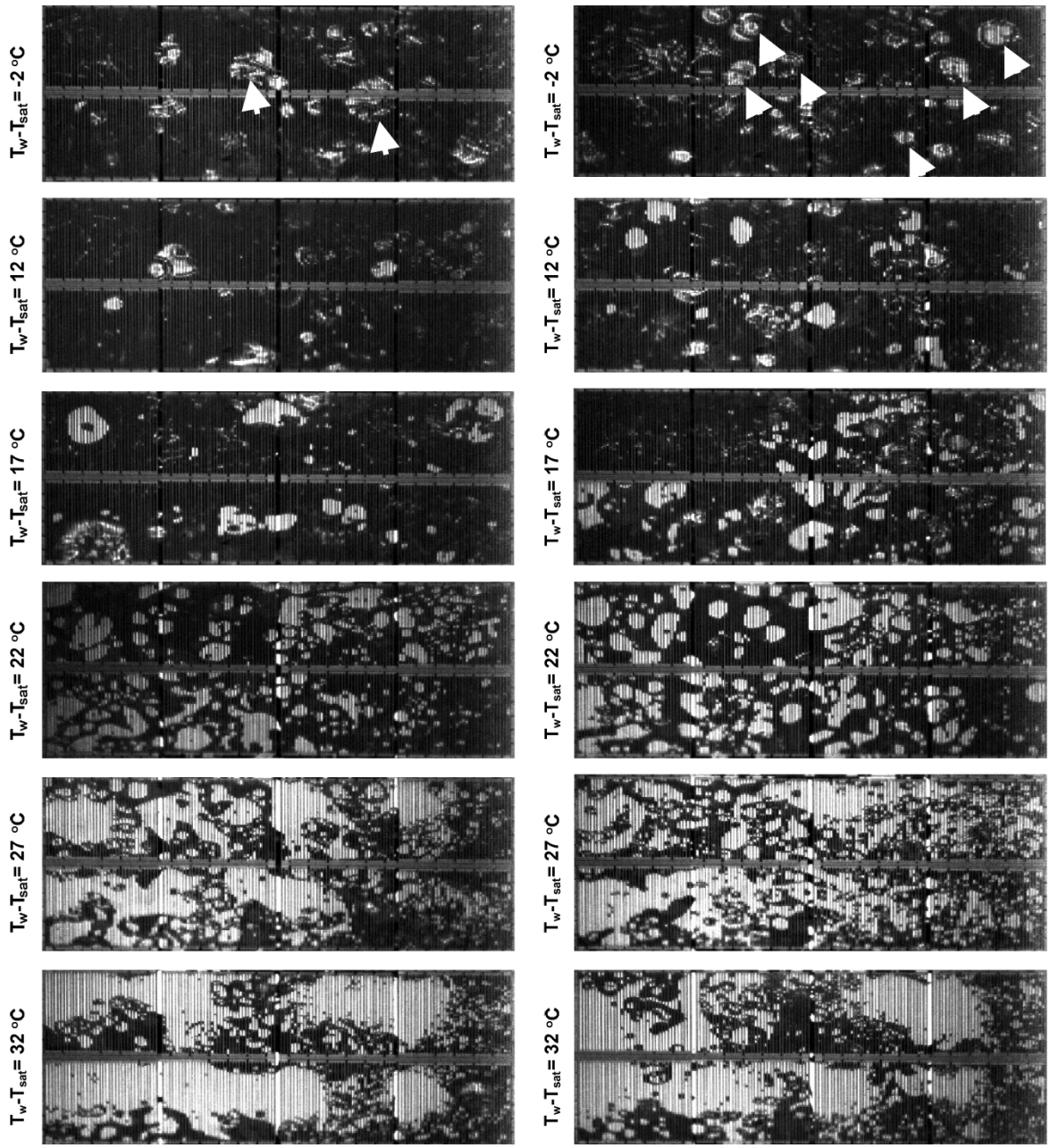

Fig. 11. (a) Single images at various surface temperatures, $h_{\mathrm{nozzle}} = 11$ mm. Single nozzle activated (case B), with nozzle axis approximately 3 heater widths beyond the right edge of image. White arrows indicate surface disturbances caused by drop impacts. (b). Single images at various surface temperatures, $h_{\mathrm{nozzle}} = 17$ mm. Single nozzle activated (case B), with nozzle axis approximately 3 heater widths beyond the right edge of image. White arrows indicate surface disturbances caused by drop impacts.

unwanted features and allowed for robust identification of wetted regions. The result of the process operated on a single heater in the array is illustrated in Fig. 12. Fig. 12(a) shows the original image obtained from the high-speed camera. A two-pixel averaging filter was convolved with the image such that the orientation of the 2-pixel stencil was orthogonal to the heater lines, resulting in each pixel averaged with the neighbor immediately above itself [Fig. 12(b)]. This has the effect of smearing out the heaters without losing significant details of the droplets. Each element (denoted by subscript i) in the line along the direction of the heater element (denoted by the subscript j) was then renormalized by the minimum and maximum intensity values contained in that individual line

$$\hat{G}_{i,j} = \frac{G_{i,j} - G_{\min,j}}{G_{\max,j} - G_{\min,j}}$$

with $G_{\min,j} = \min[G_j, 0.45]$ and $G_{\max,j} = \max[G_j, 0.65]$, resulting in a more uniform grayscale range, and tended to remove any residual variation caused by the presence of the heater element image [see Fig. 12(c)]. The final processed image was obtained by taking a threshold grayscale value to determine the boundary between the wet and dry regions of the vapor interface,

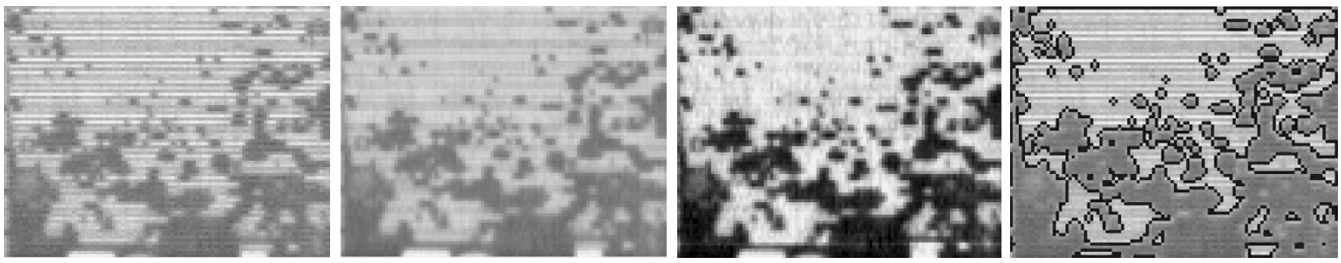

(a) (b) (c) (d)

Fig. 12. Image processing sequence. From left to right: (a) original image; (b) 2-pixel orthogonal filter applied; (c) line-by-line renormalization; (d) final detected edges (shown as black lines, representing the contact line) superimposed on original image.

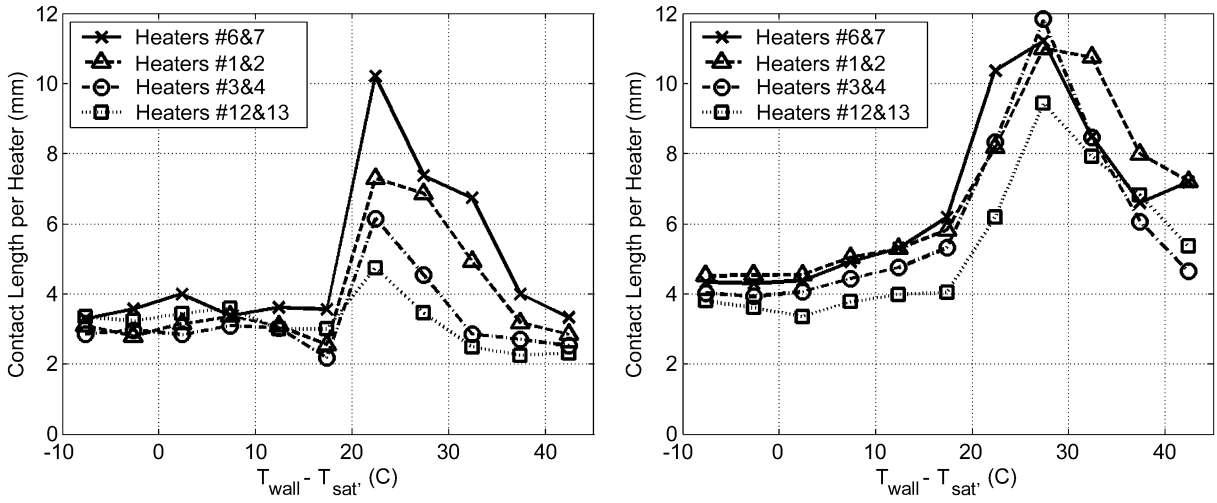

Fig. 13. Contact line length versus wall superheat for Nozzle A. (a) $h = 7$ mm. (b) $h = 17$ mm.

as shown in Fig. 12(d). Light gray patches inside and around the liquid regions were often observed. These are believed to be regions of thin fluid where the curvature is weak relative to the thickness of the film, thus reflecting some of the light from the liquid/vapor interface. It was found that setting the threshold level to a value of 0.56 easily detected these regions as wetting liquid, while still rejecting the other dry regions on the surface. The smallest features that could consistently be detected by these means were found to be around 3 to 4 pixels.

The variation in L_c for heaters across the array versus wall temperature are shown on Fig. 13 for nozzle A, $h = 7$ mm and $h = 17$ mm. The curves indicate that L_c is roughly constant for temperatures corresponding to the single phase region (wall superheats less than 17 °C), although there are variations from heater to heater. Typical values of the contact line length (L_c) are around 3–4.5 mm per heater (or normalized by the area of the individual heater elements, 6000 to 9000 m/m^2), and are most likely caused by the surface wave disturbances noted in the visualizations discussed in Section IV-C. It is less certain, however, whether or not the surface is actually dry in this region, or simply covered with an extremely thin layer of fluid which is forcing the fluid/vapor interface to be parallel to the heated substrate. Given that the apparent "dry" region of the streaks are typically 20–30 μm in width, any fluid layer present would likely have to be much thinner than this to provide a sufficiently flat interface to ensure a detectible reflection.

L_c sharply increases once the two-phase region is entered with the peak occurring at the same superheat as CHF, then decreases as the dry area fraction increases beyond CHF. For $h = 7$ mm, L_c is largest closest to the nozzle in the two phase region (heaters 6 and 7), and decreases as the distance from the spray axis increases. For $h = 17$ mm, there is much less variation in L_c among the heaters onto which the spray impacts (6 and 7, 1 and 2, and 3 and 4). Heaters 12 and 13, which are at the edge of the spray, have lower L_c.

It is apparent that L_c is strongly correlated with the phase change heat transfer. This is more clearly shown on Fig. 14 where the wall heat flux is plotted versus L_c. The contact line length is relatively independent of heat flux in the single phase region. The heaters closer to the spray axis require a higher heat flux to be reached before the two phase region is entered for $h = 7$ mm—this may be due to a higher single phase convection component for the heaters closer to the spray axis. Once the two-phase region is entered, however, L_c closely tracks the heat flux through CHF and beyond. It is also interesting to note that the slope of all of the curves is about 30 $(\mathrm{W/cm^2})/\mathrm{cm}$. Similar trends were observed for Nozzle B and Nozzles A + B.

Nishio and Tanaka [13] studied pool boiling on a sapphire substrate using ethanol, R113, and R141b. They visualized the surface using a TIR technique similar to that used in this study. Isolated circular dry areas were observed at low wall superheats, comparable to what was observed in this study. At

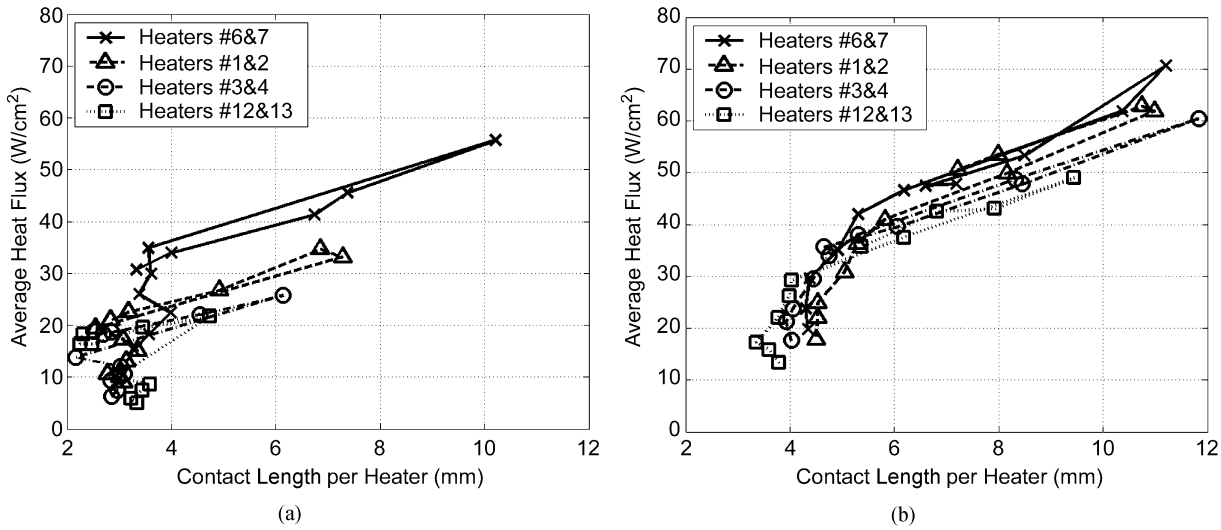

Fig. 14. Contact line length versus heat flux for Nozzle A. (a) $h = 7$ mm. (b) $h = 17$ mm.

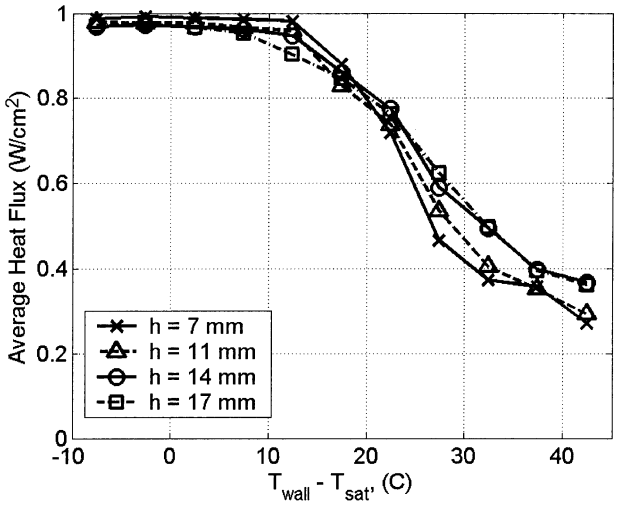

Fig. 15. Wetted area versus wall superheat, Nozzle A.

higher superheats, coalesced dry areas appeared, but "a network of liquid-solid contacts like a canal meandering between dry areas" was observed on the surface, and small circular dry areas within these liquid-solid contacts could be seen. In the current spray cooling studies, no such "canals" between dry patches were observed. In spite of the different flow structures, a strong correlation between the contact line length and heat flux was found—the contact line length increased with wall superheat, peaked at the temperature corresponding to CHF, then decreased beyond CHF.

The wetted area was observed to monotonically decrease with superheat (Fig. 15) for all cases, similar to what was previously observed [5] for cases with widely varying amounts of gas and subcooling. No correlation with the spray cooling curves is apparent. It appears the superheat determines the amount of the surface area wetted by the liquid, but not the heat flux.

V. Conclusion

The heat transfer distribution under one and two spray nozzles was measured along with visualization of the liquid-solid contact area. The main conclusions that can be made from this work are summarized.

1) A maximum heat flux of 66 W/cm^2 at a superheat of 28 °C was attained for the cases studied. This value, however, is not an upper bound to what can be obtained with spray cooling, but rather reflects the particular conditions selected for the current experiments.
2) For a given nozzle-to-surface distance, the highest heat transfer occurred directly under the spray nozzle. This is likely to be dependent on the distribution of the spray used, which was not varied in this experiment.
3) The heat flux became more uniform across the heated surface as the nozzle-to-surface distance was increased. From a design perspective, this implies that there is likely an optimum spacing for the nozzles from the heated surface if one wishes to achieve uniform heat flux distribution. This, however, may not be the same optimum if one wishes to maximize the net heat removal rate from the entire surface.
4) For a fixed nozzle-to-surface spacing, the average heat flux within the region covered by the spray is the same for both the single- and two-nozzle cases, at least within the uncertainty of the measurement (5%). This result may stem from the fact that the sprays are relatively dilute, and so have a weak influence on one another when acting in tandem (e.g., the overlap of the sprays does not occur until they are relatively far from the surface and the droplet number density is sufficiently small to prevent droplet collisions and alter the spray pattern). It should be pointed out that this conclusion is not likely to be universal, and would likely be different in much higher flowrate conditions. This presents an important area worthy of future study.
5) The current results reinforce our previous findings that heat flux in the two-phase region is directly related to the contact line length, and not to the wetted area. The implications of this conclusion are that it may be possible to improve the control and magnitude of the heat flux if one can similarly enhance and/or control the

contact line length on the heated surface. Future areas of investigation for this topic include constructing surfaces which influence the position of the contact line either through geometric structuring of the surface, or through making patterned surface coatings that selectively modify the local wetting of the surface.

ACKNOWLEDGMENT

The authors wish to express their gratitude to P. Boudreaux (LPS) for his tremendous encouragement and support throughout this study.

REFERENCES

[1] J. D. Yang, L. C. Chow, and M. R. Pais, "Nucleate boiling heat transfer in spray cooling," *J. Heat Transfer*, vol. 118, pp. 668–671, 1996.
[2] L. C. Chow, M. S. Sehmbey, and M. R. Pais, "High-heat-flux spray cooling," *Annu. Rev. Heat Transfer*, vol. 8, pp. 291–318, 1997.
[3] K. A. Estes and I. Mudawar, "Comparison of two-phase electronic cooling using free jets and sprays," *J. Electron. Packag.*, vol. 117, pp. 323–332, 1995.
[4] B. Horacek, J. Kim, and K. T. Kiger, "Effects of noncondensible gas and subcooling on the spray cooling of an isothermal surface," in *Proc. ASME IMECE*, Washington, DC, 2003, Paper IMECE2003-41680.
[5] B. Horacek, J. Kim, and K. Kiger, "Gas effects on spray cooling of an isothermal surface: visualization and time and space resolved heat transfer measurements," in *Proc. 42nd AIAA Aerospace Sciences Meeting and Exhibit*, Reno, NV, 2004.
[6] D. E. Tilton, C. L. Tilton, M. R. Pais, and M. J. Morgan, "High-flux spray cooling in a simulated multichip module," in *Proc. 1992 ASME Heat Transfer Conf.*, 1992, Paper HTD-Vol. 206-2.
[7] L. Ortiz and J. E. Gonzalez, "Experiments on steady-state high heat fluxes using spray cooling," *Experimental Heat Transfer*, vol. 12, pp. 215–233, 1999.
[8] C. M. Kendall and J. P. Holman, "Spray cooling heat-transfer with subcooled trichlorotrifluoroethane (freon-113) for vertical constant heat flux surfaces," in *Proc. ASME Heat Transfer Division*, vol. 2, 1996.
[9] R. C. Chen, L. C. Chow, and J. E. Navedo, "Effects of spray characteristics on critical heat flux in subcooled water spray cooling," *Int. J. Heat & Mass Transfer*, vol. 45, pp. 4033–4043, 2002.
[10] J. P. Holman and C. M. Kendall, "Extended studies of spray cooling with freon-113," *Int. J. Heat & Mass Transfer*, vol. 36, no. 8, pp. 2239–2241, 1993.
[11] L. Lin, R. Ponnappan, K. Yerkes, and B. Hager, "Large area spray cooling," in *Proc. 42nd AIAA Aerospace Sciences Meeting and Exhibit*, Reno, NV, 2004.
[12] S. Nishio, T. Gotoh, and N. Nagai, "Observation of boiling structures in high heat-flux boiling," *Int. J. Heat Mass Trans.*, vol. 41, pp. 3193–3201, 1998.
[13] S. Nishio and H. Tanaka, "Visualization of boiling structures in high heat-flux pool-boiling," *Int. J. Heat Mass Transfer*, vol. 47, pp. 4559–4568, 2004.
[14] A. Frohn and N. Roth, *Dynamics of Droplets*. Berlin, Germany: Springer-Verlag, 2000.
[15] I. Mudawar and K. A. Estes, "Optimizing and predicting CHF in spray cooling of a square surface," *J. Heat Transfer*, vol. 118, pp. 672–679, 1996.
[16] K. A. Estes and I. Mudawar, "Correlation of sauter mean diameter and critical heat flux for spray cooling of small surfaces," *Int. J. Heat Mass Transfer*, vol. 38, no. 16, pp. 2985–2996, 1995.

Bohumil Horacek received the Diplom-Ingenieur from Fachhochschule Mannheim—Hochschule für Technik und Gestaltung in chemical process engineering in 2002.

Following his graduation, he joined the Department of Mechanical Engineering, University of Maryland, College Park, as a Faculty Research Assistant. He is currently working as a Development Engineering for Degussa Construction Chemicals Ltd., Chrudim, Czech Republic.

Jungho Kim received the B.S.M.E. degree from the University of California, Berkeley in 1982, and the M.S.M.E. and Ph.D. degrees from the University of Minnesota, Minneapolis, in 1986 and 1990, respectively, all in mechanical engineering.

From 1990 to 1992, he was with Arvin/Calspan Corporation, Buffalo, NY, where he performed research in gas turbine heat transfer. From 1992 to 1998, he taught at the University of Denver, where he started research on gravity effects on boiling heat transfer using a microheater array. He joined the faculty at the University of Maryland in 1998. His current research interests are phase change heat transfer for electronic cooling, radiation absorption measurements of fuels at high temperatures, emissivity measurements, inverse heat conduction methods, and instrumentation. He has published over 70 technical papers.

Kenneth T. Kiger was received the B.S.A.E. degree from the University of Southern California, Los Angeles, in 1991, and the M.S.A.E. and Ph.D. degrees in applied mechanics from the University of California, San Diego, in 1993 and 1995, respectively.

After completing his graduate studies, he joined the faculty in the Department of Mechanical Engineering, University of Maryland, College Park, in 1995. His research interests encompass a broad range of fluid mechanics and heat transfer, with a specialization in multiphase flows, sprays and optic-based instrumentation. He has published over 40 technical papers.